Theoretical Study of Bimolecular Nucleophilic Substitution at Four-, Five-, and Six-Coordinate Metal Carbonyl Radicals

Michael J. Therien and William C. Trogler*

Contribution from the Department of Chemistry, D-006, University of California at San Diego, La Jolla, California 92093. Received November 23, 1987

Abstract: Walsh diagrams, contour maps, and the atomic character and energies of the frontier molecular orbitals derived from SCF–Xα–DV calculations have been employed to deduce the most favorable mode of nucleophilic attack at homoleptic metal carbonyl radicals constrained to ideal octahedral, trigonal-bipyramidal, square-pyramidal, and tetrahedral geometries. These studies show that two-center three-elelctron bonding may stabilize a hypervalent 19-electron (19e) transition state or intermediate formed during nucleophilic attack. Spin-polarized calculations suggest a difference between these 19e species and those formed via reduction of saturated, 18e organometallics. For example, little spin density is calculated to delocalize onto the CO ligands when a nucleophile attacks $Mn(CO)_5$ to form a 19e complex. Nucleophilic attack at a face, rather than at an edge of an octahedron, is predicted for the 17e complex $V(CO)_6$. Nucleophilic attack at the open face of the square pyramid is the only mode of attack (of six available) that can be stabilized by two-center three-electron bonding for the square-pyramidal 17e complex $Mn(CO)_5$. Preferred attack at an edge in the equatorial plane is predicted for the trigonal-bipyramidal 17e radical $Mn(CO)_5$. Attack at a tetrahedral face, analogous to S_N2 substitution at carbon, is predicted for the tetrahedral 17e species $Co(CO)_4$.

Recent studies of carbonyl-containing 17-electron (17e) organometallic radicals[1–21] have shown that these species are exceptionally labile and that they can participate in a variety of catalytic and stoichiometric transformations, which include nucleophile-induced carbonyl insertion[18–20] and ligand substitution.[1–18] The enhanced reactivity observed at paramagnetic metal carbonyl centers has led to speculation[1,19,20] that these species may function as intermediates in catalytic cycles.

Substitution lability represents a key feature of 17e metal carbonyl radicals. For example, it has been shown that 17e V(0) and Fe(I) carbonyl complexes substitute CO 10^9–10^{10} times faster than analogous 18e complexes.[7,17] A large body of evidence[3c,d,6,7,9–11,12a,14–17] suggests that substitution reactions of 17e metal carbonyl radicals are associative. This associative reactivity presumably requires nucleophilic attack at the metal radical center to produce a 19e intermediate or transition state, and uncertainty remains about the structure of these 19e intermediates and the origin of the rate acceleration. Since two-center three-electron bonding[7] has been proposed to stabilize such a species, we have performed theoretical calculations to test this hypothesis for several possible modes of nucleophilic attack at simple polyhedral metal carbonyl radical complexes.

Total energies are only beginning to be obtained[22] for transition-metal complexes using the Xα method; however, their application to complex potential surfaces has not yet been realized. Therefore, the approach taken in this paper utilizes SCF–Xα–DV calculations to depict frontier orbital interactions. First, we determine whether the proposed two-center three-electron bond forms at reasonable metal–nucleophile distances, without relaxation of the metal radical geometry. We then qualitatively evaluate the most favorable mode of nucleophilic attack at six-, five-, and four-coordinate homoleptic metal carbonyl radical centers. Our analysis relies purely on electronic effects. Steric effects in specific complexes may temper the general predictions. Because electronic effects must be responsible for the 10^{10} increase of associative

(1) (a) Brown, T. L. *Ann. N.Y. Acad. Sci. U.S.A.* **1980**, *333*, 80. (b) Halpern, J. *Pure Appl. Chem.* **1986**, *58*, 575. (c) Kochi, J. K. *Organometallics Mechanisms and Catalysis*; Academic: New York, 1978. (d) Collman, J. P.; Hegedus, L. S.; Norton, J. R.; Finke, R. G. *Principles and Applications of Organotransition Metal Chemistry*; University Science Books: Mill Valley, CA, 1987. (e) Lappert, M. F.; Lednor, P. W. *Adv. Organomet. Chem.* **1976**, *14*, 345. (f) Kochi, J. K. *J. Organomet. Chem.* **1986**, *300*, 139. (g) Trogler, W. C. *Int. J. Chem. Kinet.* **1987**, *19*, 1025.

(2) Darchen, A.; Mahé, C.; Patin, H. *J. Chem. Soc., Chem. Commun.* **1982**, 243.

(3) (a) Bezems, G. J.; Rieger, P. H.; Visco, S. J. *J. Chem. Soc., Chem. Commun.* **1981**, 265. (b) Hershberger, J. W.; Kochi, J. K. *J. Chem. Soc., Chem. Commun.* **1982**, 212. (c) Hershberger, J. W.; Klinger, R. J.; Kochi, J. K. *J. Am. Chem. Soc.* **1982**, *104*, 3034. (d) Zizelman, P. M.; Amatore, C.; Kochi, J. K. *Ibid.* **1984**, *106*, 3771. (e) Narayanan, B. A.; Kochi, J. K. *J. Organomet. Chem.* **1984**, *272*, C49.

(4) Kinney, R. J.; Jones, W. D.; Bergman, R. G. *J. Am. Chem. Soc.* **1978**, *100*, 7902.

(5) Schroder, N. C.; Angelici, R. J. *J. Am. Chem. Soc.* **1986**, *108*, 3688.

(6) (a) Stiegman, A. E.; Goldman, A. S.; Leslie, D. B.; Tyler, D. R. *J. Chem. Soc., Chem. Commun.* **1984**, 632. (b) Stiegman, A. E.; Stieglitz, M.; Tyler, D. R. *J. Am. Chem. Soc.* **1983**, *105*, 6032. (c) Goldman, A. S.; Tyler, D. R. *Ibid.* **1984**, *106*, 4066. (d) Stiegman, A. E.; Tyler, D. R. *Inorg. Chem.* **1984**, *23*, 527.

(7) (a) Shi, Q.-Z.; Richmond, T. G.; Trogler, W. C.; Basolo, F. *J. Am. Chem. Soc.* **1984**, *106*, 71. (b) Richmond, T. G.; Shi, Q.-Z.; Trogler, W. C.; Basolo, F. *J. Am. Chem. Soc.* **1984**, *106*, 76.

(8) (a) Kowaleski, R. M.; Basolo, F.; Trogler, W. C.; Ernst, R. D. *J. Am. Chem. Soc.* **1986**, *108*, 6046. (b) Kowaleski, R. M.; Trogler, W. C.; Basolo, F. *Gazz. Chim. Ital.* **1986**, *116*, 105. (c) Kowaleski, R. M.; Basolo, F.; Osborne, J. H.; Trogler, W. C. *Organometallics*, in press.

(9) Downard, A. J.; Robinson, B. H.; Simpson, J. *Organometallics* **1986**, *5*, 1140.

(10) (a) Fox, A.; Malito, J.; Poé, A. *J. Chem. Soc., Chem. Commun.* **1980**, 1052. (b) Fawcett, J. P.; Jackson, R. A.; Poé, A. *Ibid.* **1975**, 733. (c) Poé, A.; Sekbar, C. B. *J. Am. Chem. Soc.* **1985**, *107*, 4874.

(11) Natalyia, N. N.; Huggins, J. M. *Organometallics* **1986**, *5*, 1703.

(12) (a) Herrinton, T. R.; Brown, T. L. *J. Am. Chem. Soc.* **1985**, *107*, 5700. (b) Wegman, R. W.; Olson, R. J.; Gard, D. R.; Faulkner, L. R.; Brown, T. L. *Ibid.* **1981**, *103*, 6089. (c) McCullen, S. B.; Brown, T. L. *Ibid.* **1982**, *104*, 7496. (d) McCullen, S. B.; Walker, H. W.; Brown, T.L. *Ibid.* **1982**, *104*, 4007. (e) Wegman, R. W.; Brown, T. L. *Organometallics* **1982**, *1*, 47. (f) Walker, H. W.; Herrick, R. S.; Olson, R. J.; Brown, T. L. *Inorg. Chem.* **1984**, *23*, 3748. (g) Lee, K.-W.; Brown T. L. *J. Am. Chem. Soc.* **1987**, *109*, 3269.

(13) (a) Bagchi, R. N.; Bond, A. M.; Colton, R.; Luscombe, D. L.; Moir, J. E. *J. Am. Chem. Soc.* **1986**, *108*, 3352. (b) Bond, A. M.; Colton, R.; McGregor, K. *Inorg. Chem.* **1986**, *25*, 2378.

(14) (a) Wrighton, M. S.; Ginley, D. S. *J. Am. Chem. Soc.* **1975**, *97*, 2065. (b) Hepp, A. F.; Wrighton, M. S. *Ibid.* **1983**, *105*, 5935. (c) Hepp, A. F.; Wrighton, M. S. *Ibid.* **1981**, *103*, 1258.

(15) Doxsee, K. M.; Grubbs, R. H.; Anson, F. C. *J. Am. Chem. Soc.* **1984**, *106*, 7819.

(16) Krusic, P. J.; Briere, R.; Rey, P. *Organometallics* **1985**, *4*, 801.

(17) Therien, M. J.; Ni, C.-L.; Anson, F. C.; Osteryoung, J. G.; Trogler, W. C. *J. Am. Chem. Soc.* **1986**, *108*, 4037.

(18) (a) Magnuson, R. H.; Zulu, S.; T'sai, W.-M.; Giering, W. P. *J. Am. Chem. Soc.* **1980**, *102*, 6887. (b) Magnuson, R. H.; Meirowitz, R.; Zulu, S. Giering, W. P. *J. Am. Chem. Soc.* **1982**, *104*, 5790. (c) Magnuson, R. H.; Meirowitz, R.; Zulu, S. Giering, W. P. *Organometallics* **1983**, *2*, 460.

(19) Therien, M. J.; Trogler, W. C. *J. Am. Chem. Soc.* **1987**, *109*, 5127.

(20) (a) Feder, H. M.; Halpern, J. *J. Am. Chem. Soc.* **1975**, *97*, 7187. (b) Sweany, R.; Halpern, J. *Ibid.* **1977**, *99*, 8335. (c) Rathke, J. W.; Feder, H. M. *J. Am. Chem. Soc.* **1978**, *100*, 3623. (d) Azran, J.; Orchin, M. *Organometallics* **1984**, *3*, 197.

(21) Greiser, T.; Puttfarcken, U.; Rehder, D. *Transition Met. Chem. (N.Y.)* **1979**, *4*, 168. Rehder, D.; Muller, I.; Kopf, J. *J. Inorg. Nucl. Chem.* **1978**, *40*, 1013.

(22) (a) Ziegler, T.; Tschinke, V.; Becke, A. *J. Am. Chem. Soc.* **1987**, *109*, 1351. (b) Ziegler, T.; Versluis, L.; Tschinke, V. *J. Am. Chem. Soc.* **1986**, *108*, 612. (c) Ziegler, T.; Tschinke, V.; Ursenbach, C. *J. Am. Chem. Soc.* **1987**, *109*, 4825, and references cited therein.

Metal Carbonyl Radicals

J. Am. Chem. Soc., Vol. 110, No. 15, 1988 4943

Table I. Atomic Character of Frontier Orbitals for Facial PH$_3$ Attack at V(CO)$_6$ (Vanadium-Phosphorus Distance 3.5 Å)

orbital	energy,[a] eV	orbital character	% contribution from atoms						
			V	C[c]	C[d]	O[c]	O[d]	P	H
17e	-1.49	d$_{x^2-y^2}$, d$_{xy}$, d$_{xz}$, d$_{yz}$	51	13	13	6	8	9	0
13a$_1$	-2.03	d$_{z^2}$	32	23	19	14	8	3	1
16e	-2.14	d$_{x^2-y^2}$, d$_{xy}$, d$_{xz}$, d$_{yz}$	39	19	19	10	11	1	1
4a$_2$	-2.37		0	39	26	22	14	0	0
15e	-2.49		1	29	31	17	19	1	1
3a$_2$	-3.21		0	24	40	14	22	0	0
14e	-3.33		0	33	28	19	17	1	2
12a$_1$	-3.60		2	28	32	14	18	4	1
13e	-3.71		1	31	34	16	18	0	0
11a$_1$[b]	-6.69	d$_{z^2}$	62	6	9	6	11	5	1
12e	-6.77	d$_{x^2-y^2}$, d$_{xy}$, d$_{xz}$, d$_{yz}$	61	9	10	9	10	0	0
10a$_1$	-9.05		2	15	2	10	1	62	9
11e	-11.15		1	40	16	17	8	7	10
9a$_1$	-11.41		1	31	33	17	13	5	0
10e	-11.81		3	3	24	5	10	27	28
9e	-12.14		19	22	21	10	9	11	8
2a$_2$	-13.00		0	4	18	13	66	0	0
8e	-13.02		0	4	20	12	65	0	0
1a$_2$	-13.07		0	20	3	65	12	0	0
7e	-13.15		0	2	25	6	66	1	0

[a] From spin-restricted calculations. [b] Denotes highest occupied orbital. [c] Denotes atom occupying the face where the nucleophile attacks. [d] Denotes atom occupying the face trans to where the nucleophile attacks.
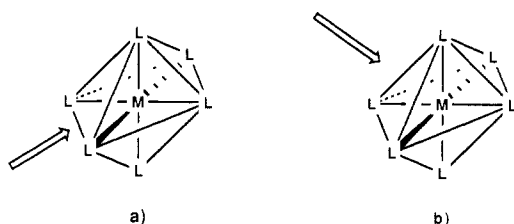

Figure 1. Two possible modes of nucleophilic attack at an octahedral ML$_6$ metal radical complex: (a) nucleophilic attack along a vector bisecting an edge and (b) nucleophilic attack along a vector passing through the center of an octahedral face.

ligand substitution rates observed for 17e V(CO)$_6$ as compared to those of 18e Cr(CO)$_6$, this latter limitation should not be serious.

Results and Discussion

Hexacoordinate Metal Carbonyl Radicals. Two modes of nucleophilic attack can be envisioned for an octahedral ML$_6$ complex: (a) attack along a vector bisecting an edge defined by two ligands; (b) attack along a vector passing through the center of an octahedral face defined by the ligands (Figure 1). The approach taken in this study is to bring the 2e donor PH$_3$ ligand toward the hexacoordinate metal radical V(CO)$_6$ from a distance where no electronic interaction occurs ($\sim$9 Å) to a distance where appreciable electronic interaction occurs ($\sim$2.6 Å). Results of electronic structure calculations for edge and facial attack of PH$_3$ at V(CO)$_6$ for a variety of distances between 9 and 2.6 Å are summarized in the Walsh diagrams of Figures 2 and 3.

Nucleophilic attack at a face of the octahedral metal radical produces a hypervalent heptacoordinate species possessing a monocapped trigonal-prismatic structure (C_{3v} symmetry). Figure 2 contains the Walsh diagram obtained for such a hypothetical reaction pathway. At a metal–phosphorus bond distance of 9.0 Å, the three highest energy frontier orbitals are the partially filled d(t_{2g}^5) set, which are split into 12e and 11a$_1$ by the reduced C_{3v} symmetry of the reaction coordinate, and the filled 10a$_1$ phosphorus lone-pair orbital. As the PH$_3$ molecule approaches the vanadium nucleus along a vector through the center of an octahedral face, appreciable electronic interaction occurs between the two species. While the orthogonal 12e orbital remains of metal–carbon π bonding and CO π^* character, the 10a$_1$ phosphorus lone-pair orbital becomes increasingly metal–phosphorus σ bonding in character with decreasing metal–phosphorus distance and the 11a$_1$ metal d orbital acquires metal–phosphorus σ^* character. The electronic configuration 10a$_1$^{2}12e^{4}11a$_1$^{1} becomes favored at vanadium–phosphorus distances below 3.75 Å. The putative hep-
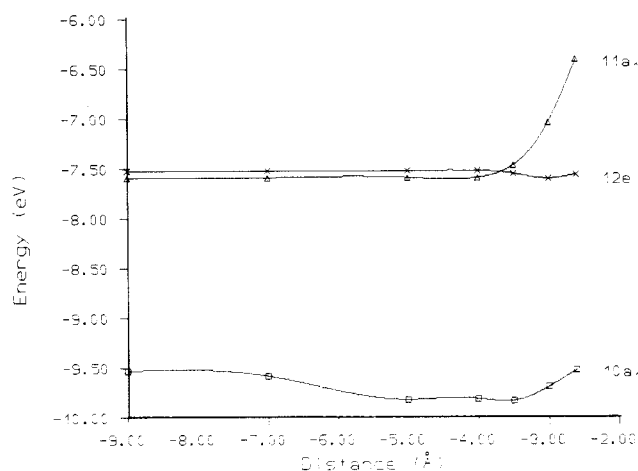
Figure 2. Walsh diagram showing the relative energies of the 10a$_1$, 12e, and 11a$_1$ orbitals for PH$_3$ attack at the center of an octahedral face of V(CO)$_6$ as the metal–nucleophile distance decreases from 9.0 to 2.6 Å.

tacoordinate transition-state structure exhibits a net metal–phosphorus bond order of $^1/_2$. The development of appreciable V–P bonding at distances as large as 3.5 Å, well beyond the normal V–P bond length of 2.45 Å,[21] suggests that our inability to allow changes in the geometry at the metal center (i.e. no total energy minimization) does not hinder analysis of the frontier orbital interactions. Note in Figure 2 that the metal–phosphorus 10a$_1$ orbital exhibits a broad bonding minimum. Table I gives orbital energies and atomic character of the frontier molecular orbitals for facial attack at a distance of 3.5 Å, and data for other distances are available as supplementary material. Analogous calculations for the approach of PH$_3$ to Cr(CO)$_6$ show similar orbital interactions, except the 10a$_1$^{2}12e^{4}11a$_1$^{2} electronic configuration has a net Cr–P bond order of 0. Thus, nucleophilic attack at an 18e metal complex is unfavorable (σ^* orbitals are more antibonding than the corresponding σ bond). As a consequence 18e complexes usually react by ligand dissociation[23a] unless certain ligands are present (e.g. cyclopentadienyl)[23b] that stabilize an excess electron count. The hypothesis that a two-center three-electron bond forms between a 17e metal radical and a nucleophile to diminish the

(23) (a) Basolo, F.; Pearson, R. G. *Mechanisms of Inorganic Reactions*; Wiley: New York, 1967. (b) Basolo, F. *Inorg. Chim. Acta* **1985**, *100*, 33. (c) Spees, S. T., Jr.; Perumareddi, J. R.; Adamson, A. W. *J. Am. Chem. Soc.* **1968**, *90*, 6626. (d) Thompson, H. B.; Bartell, L. S. *Inorg. Chem.* **1968**, *7*, 488.

Table II. Atomic Character of Frontier Orbitals for Edge PH$_3$ Attack at V(CO)$_6$ (Vanadium–Phosphorus Distance 3.5 Å)

orbital	energy, eV	orbital character	V	C^b	O^b	C^c	O^c	C^d	O^d	C^d	O^d	P	H^e	H
21a''	-1.06	d$_{yz}$,d$_{xz}$	44	20	7	19	7	0	0	0	0	1	2	0
30a'	-1.16	d$_{z^2}$, d$_{x^2-y^2}$, d$_{xy}$	40	7	2	7	2	10	4	8	4	15	0	0
29a'	-1.54	d$_{z^2}$, d$_{x^2-y^2}$, d$_{xy}$	37	18	11	12	6	4	2	4	2	3	1	1
28a'	-1.60	d$_{z^2}$, d$_{x^2-y^2}$, d$_{xy}$	31	6	4	5	2	20	10	11	5	3	1	1
20a''	-1.61	d$_{yz}$, d$_{xz}$	32	7	3	7	3	21	10	13	5	0	0	0
19a''	-1.94		3	19	13	14	9	18	10	9	4	0	0	0
27a'	-2.00		8	18	13	16	12	14	7	8	3	0	1	1
18a''	-2.25		1	28	15	35	19	0	0	0	0	1	1	0
26a'	-2.74		2	11	6	17	11	11	7	19	13	2	0	0
17a''	-2.83		1	11	5	9	4	16	10	27	18	0	0	0
16a''	-2.90		0	29	16	34	20	0	0	1	0	0	0	0
25a'	-3.18		3	15	7	18	9	12	7	16	9	3	1	0
24a'	-3.40		0	26	16	28	17	5	0	5	1	0	0	0
15a''	-3.44		2	28	14	24	11	5	3	9	5	0	0	0
23a'^{a}	-6.20	d$_{z^2}$, d$_{x^2-y^2}$, d$_{xy}$	58	8	4	12	11	0	0	0	0	6	1	1
14a''	-6.27	d$_{yz}$, d$_{xz}$	62	4	5	6	5	3	5	5	5	0	0	0
22a'	-6.29	d$_{z^2}$, d$_{x^2-y^2}$, d$_{xy}$	62	4	5	5	5	4	5	5	5	0	0	0
21a'	-8.13	d$_{z^2}$, d$_{x^2-y^2}$, d$_{xy}$	2	15	21	1	1	0	0	0	0	50	6	3
13a''	-10.41		1	24	16	7	2	0	1	0	1	17	31	0
20a'	-10.83		1	0	6	0	4	33	11	36	10	0	0	0
19a'	-10.96		0	32	16	31	11	0	4	0	2	3	0	0
18a'	-11.22		0	2	4	0	0	0	0	0	0	49	15	29
12a''	-11.23		1	17	5	34	11	1	6	0	2	13	12	0
17a'	-11.64	d$_{z^2}$, d$_{x^2-y^2}$, d$_{xy}$	26	8	3	9	3	16	11	15	8	1	0	0
11a''	-11.65	d$_{yz}$, d$_{xz}$	24	28	13	21	9	0	0	0	0	3	2	0

^{a} Denotes highest occupied orbital. ^{b} Denotes atoms defining edge where nucleophile attacks. ^{c} Denotes atoms defining edge trans to where nucleophile attacks. ^{d} Denotes axial atoms. ^{e} Denotes hydrogens related by the mirror plane.
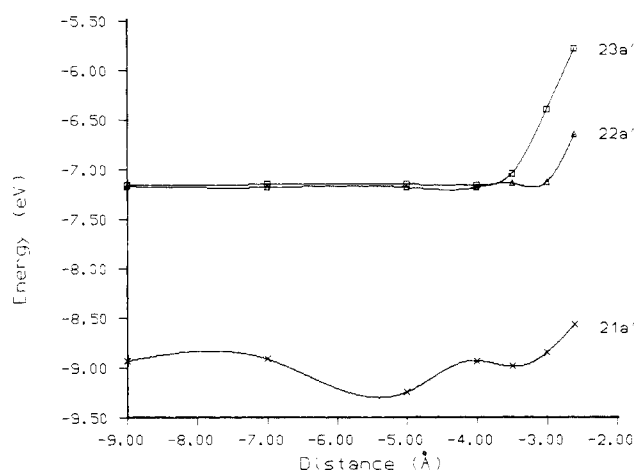
Figure 3. Walsh diagram showing the relative energies of the 21a', 22a', and 23a' orbitals for PH$_3$ attack at an octahedral edge of V(CO)$_6$ as the metal–nucleophile distance decreases from 9.0 to 2.6 Å.

activation barrier for an associative reaction path therefore finds support from a consideration of the frontier orbital interactions. If the bonding is strong enough, then the 19e species may be a metastable intermediate.[19]

In contrast to facial attack, approach along a vector bisecting an octahedral edge results in a pentagonal-bipyramidal structure. The Walsh diagram for this reaction path is shown in Figure 3. The three frontier orbitals of interest are 21a', 22a', and 23a'. As the nucleophile approaches the metal center the orbital character of 23a' changes from metal d to metal–phosphorus σ^*, while 21a' changes from a phosphorus lone-pair orbital to a metal–phosphorus σ bonding orbital. The 22a' orbital remains chiefly metal–carbon π and CO π^* in character. Below a 3.75-Å separation the electronic configuration 21a'^{2}22a'^{2}14a''^{2}23a'^{1} becomes favored. Again, the metal–phosphorus bond in the hypothetical hepta-coordinate transition state is of 0.5 order. Table II gives orbital energies and atomic character of the frontier molecular orbitals for edge attack at 3.5 Å, and data for other distances are available as supplementary material.

Comparison of the Walsh diagrams for facial and edge PH$_3$ attack at V(CO)$_6$ shows that the metal–phosphorus bonding orbital

for facial attack (10a$_1$) produces a more bonding potential at close V–P distances (<4 Å) than the analogous orbital for edge attack (21a'). On the basis of the Walsh diagrams, we expect that nucleophilic attack at a hexacoordinate metal radical center occurs preferentially at a face rather than at an edge of the octahedron. That facial attack yields a more favorable V–P interaction may also be seen in orbital contour plots.

Contour plots of the 10a$_1$ and 11a$_1$ orbitals for facial attack at several vanadium–PH$_3$ distances are shown in Figure 4. Figure 4A begins with the 10a$_1$ and 11a$_1$ orbitals at a metal–nucleophile distance of 9 Å, where 10a$_1$ consists exclusively of phosphorus lone-pair character and 11a$_1$ is a t$_{2g}$-derived d orbital on vanadium. Parts B–D of Figure 4 move the nucleophile closer to the metal center (from 7.0 to 3.5 Å). As the metal–nucleophile distance decreases, more metal t$_{2g}$ (d$_{xz}$, d$_{yz}$) character mixes into the 10a$_1$ orbital, while 11a$_1$ acquires phosphorus lone-pair character. Parts E and F of Figure 4 clearly show the formation of a metal–nucleophile bond in 10a$_1$. The half-filled 11a$_1$ orbital becomes metal–nucleophile antibonding.

Contour plots obtained of 21a' and 23a', the metal–nucleophile bonding and antibonding orbitals, respectively, for edge attack at an octahedral metal radical, contrast with those presented in Figure 4 for nucleophilic attack at a face. Figure 5A presents contour plots for the 21a' and 23a' orbitals at a vanadium–PH$_3$ distance of 9 Å, a distance again where the orbital is composed exclusively of phosphorus lone-pair character and where 23a' is metal d. Like parts B–D of Figure 4, increased mixing of metal d character into the orbital can be observed in parts B–D of Figure 5. Parts E and F of Figure 5, however, which give contour plots of the 21a$_1$' orbital at vanadium–phosphorus distances of 3.0 and 2.6 Å, show less overlap between the metal and the entering nucleophile than for facial attack. Note that 23a' shows similar destabilizing characteristics as 11a' did for facial attack. Thus, the contour plots suggest that nucleophilic attack at a hexa-coordinate metal radical should be slightly more favored along an octahedral face than along an edge of an octahedron.

For nucleophilic substitution reactions occurring at diamagnetic octahedral transition-metal centers, the difference between edge and facial attack is also small. Both monocapped trigonal-prismatic and pentagonal-bipyramidal transition states are considered reasonable on the basis of crystal field calculations.[23] Often a soft potential energy surface connects the ground-state diamagnetic structures of a pentagonal bipyramid and monocapped trigonal
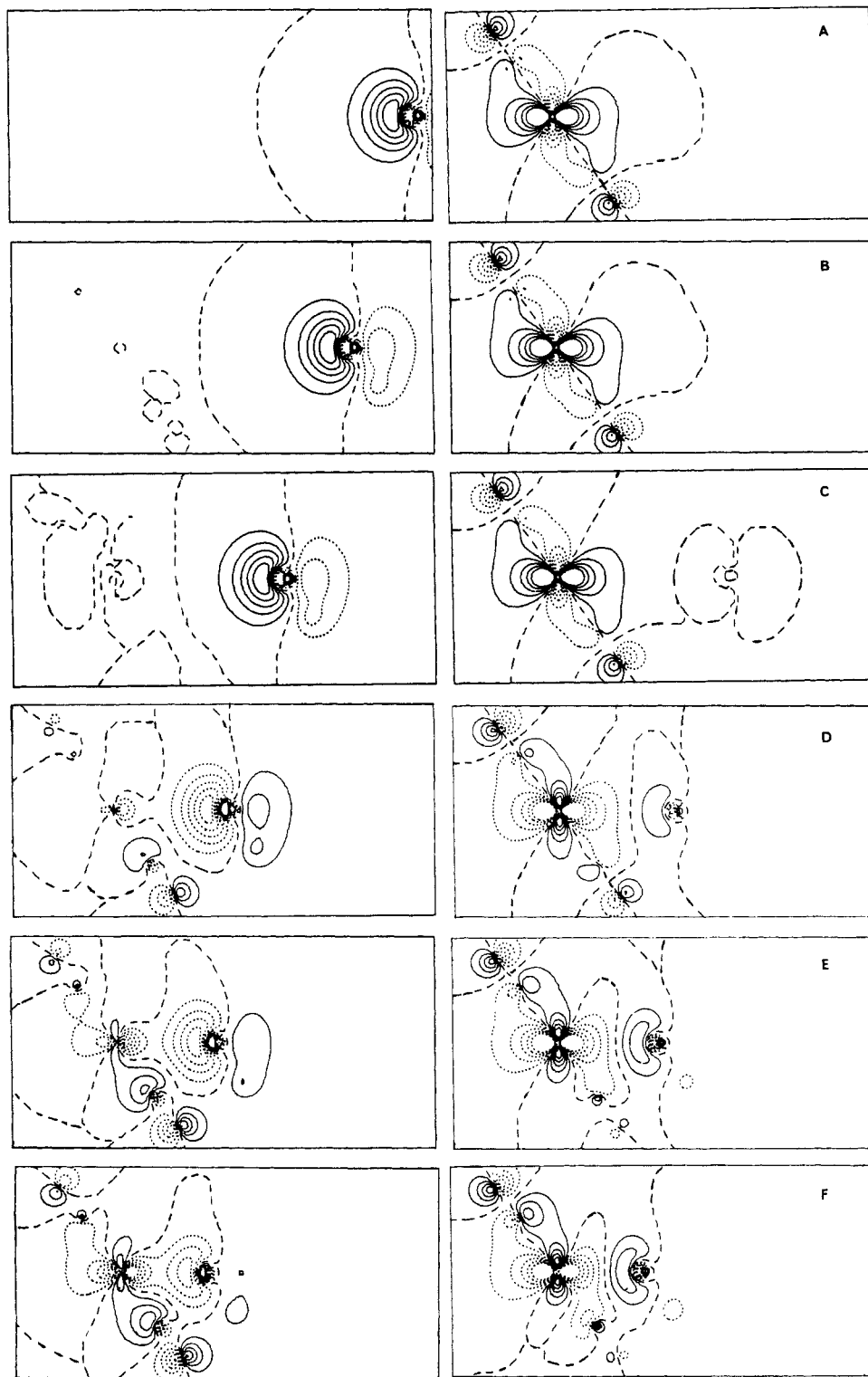
Metal Carbonyl Radicals

J. Am. Chem. Soc., Vol. 110, No. 15, 1988 4945

Figure 4. Contour plots of the $10a_1$ (left column) and $11a_1$ (right column) orbitals for facial PH_3 attack at $V(CO)_6$ at various metal–nucleophile distances: (a) 9.0, (b) 7.0, (c) 5.0, (d) 3.5, (e) 3.0, and (f) 2.6 Å. The interval between successive contours is 0.270 $e/Å^3$. Dashed lines represent the zero-level contour.

prism;[24] this is exemplified by $Mo(CN)_7^{4-}$, which exists in both geometries.[25]

Pentacoordinate Metal Carbonyl Radicals. Five-coordinate homoleptic metal carbonyl radicals are nonpersistent species.[1]

Their high reactivity often results in dimerization reactions to form metal–metal-bonded complexes,[12,14] atom-transfer reactions with various substrates,[12] and disproportionation.[26a] Because these species are short-lived, there is little structural and spectroscopic information available about them and much interest in the nature of their ground-state structures.[12f,14c,26–30] The complexes Mn-

(24) (a) Hoffmann, R.; Beier, B. F.; Muetterties, E. L.; Rossi, A. R. *Inorg. Chem.* **1977**, *16*, 511. (b) Hush, N. S. *Aust. J. Chem.* **1962**, *15*, 378. (c) Pauling, L. *Proc. Natl. Acad. Sci. U.S.A.* **1976**, *73*, 1403. (d) Wasson, J. R.; Lorenz, D. R. *Inorg. Nucl. Chem. Lett.* **1975**, *11*, 617. (e) Oakland, R. L.; Duffey, G. H. *J. Chem. Phys.* **1967**, *46*, 19. (f) Levenson, R. A.; Dominguez, R. J. G. *Inorg. Chem.* **1973**, *12*, 2342.

(25) Rossman, G. R.; Tsay, F.-D.; Gray, H. B. *Inorg. Chem.* **1973**, *12*, 824.

(26) (a) Therien, M. J.; Trogler, W. C. *J. Am. Chem. Soc.* **1986**, *108*, 3697. (b) Therien, M. J. Ph.D. Thesis, University of California, San Diego.

(27) Hughey, J. L.; Anderson, C. P.; Meyer, T. J. *J. Organomet. Chem.* **1977**, *125*, C49.
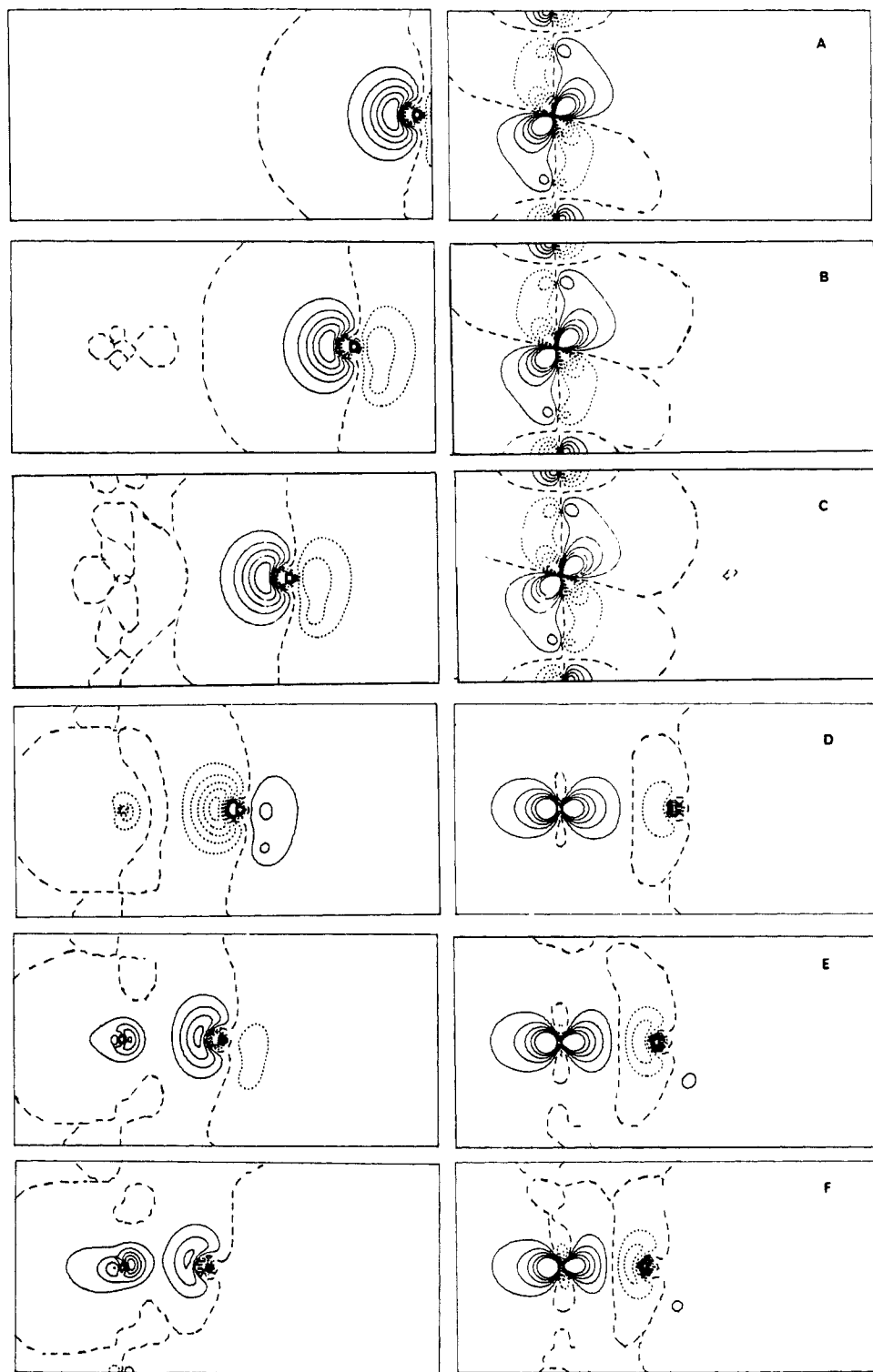
Figure 5. Contour plots of the 21a′ (left column) and 23a′ (right column) orbitals for edge PH_3 attack at $V(CO)_6$ at various metal–nucleophile distances: (a) 9.0, (b) 7.0, (c) 5.0, (d) 3.5, (e) 3.0, and (f) 2.6 Å. The interval between successive contours is 0.270 e/Å^3.

$(CO)_5$ and $Fe(CO)_3L_2^+$ represent two examples of this class of compounds. Spectroscopic studies of 17e $Mn(CO)_5$, generated in $Cr(CO)_6$ crystals or in low-temperature solid matrices, support

(28) Waltz, W. L.; Hackelberg, O.; Dorfman, L. M.; Wojcicki, A. *J. Am. Chem. Soc.* **1978**, *100*, 7259.

(29) (a) Church, S. P.; Poliakoff, M.; Timney, J. A.; Turner, J. J. *J. Am. Chem. Soc.* **1981**, *103*, 7515. (b) Symons, M. C. R.; Sweany, R. L. *Organometallics* **1982**, *1*, 834. (c) Fairhurst, S. A.; Morton, J. R.; Perutz, R. N.; Preston, K. F. *Organometallics* **1984**, *3*, 1389. (d) Howard, J. A.; Morton, J. R.; Preston, K. F. *Chem. Phys. Lett.* **1981**, *83*, 226. (e) Lionel, T.; Morton, J. R.; Preston, K. F. *Chem. Phys. Lett.* **1981**, *81*, 17.

(30) Baker, P. K.; Connelly, N. G.; Jones, B. M. R.; Maher, J. P.; Somers, K. R. *J. Chem. Soc., Dalton Trans.* **1980**, 479.
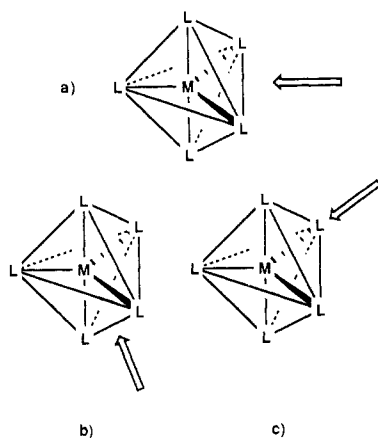
a C_{4v} (square-pyramidal) structure,[27-29] while spectroscopic studies of isoelectronic $Fe(CO)_3L_2^+$ cation radicals in solution support a D_{3h} (trigonal-bipyramidal) structure.[26,30] Nucleophilic attack at pentacoordinate metal carbonyl radicals possessing both D_{3h} and C_{4v} geometries will therefore be examined.

We consider $Mn(CO)_5$ as the archetypal pentacoordinate metal radical (idealized to D_{3h} and C_{4v} symmetries) with PH_3 as the model nucleophile. Instead of carrying out electronic structure calculations at varying metal–nucleophile distances and constructing Walsh diagrams for each of the modes of nucleophilic attack at ML_5 centers, we rely on contour plots and the atomic character and energies of the frontier orbitals obtained at a metal–nucleophile distance of 3.0 Å (where metal–nucleophile

Metal Carbonyl Radicals

J. Am. Chem. Soc., Vol. 110, No. 15, 1988 4947

Figure 6. Three possible modes of nucleophilic attack at a trigonal-bi-pyramidal ML_5 metal radical complex: (a) attack along a vector bi-secting an edge defined by two equatorial ligands (EE attack), (b) attack along a vector bisecting an edge defined by an axial and an equatorial ligand (AE attack), and (c) attack along a vector passing through the center of a trigonal-bipyramidal face (FAC attack).

electronic interactions begin to become appreciable but steric effects are diminished) to evaluate which mode of nucleophilic attack occurs. Note that using this abbreviated approach still drives one to the conclusion that facial attack is favored over edge attack at ML_6 radical centers (vide supra). As will be seen, the choice is more clear for the other structures examined.

Nucleophiles can attack a trigonal-bipyramidal complex in three general ways: (a) along a vector bisecting an edge defined by two equatorial ligands; (b) along a vector bisecting an edge defined by an axial and an equatorial ligand; (c) along a vector passing through the center of a trigonal-bipyramidal face defined by an axial and two equatorial ligands (Figure 6). All the models for hexacoordinate hypervalent transition states shown in Figure 6 possess C_s symmetries (again, PH_3 is considered to be the entering nucleophile).

The odd electron in a 17e D_{3h} ML_5 complex resides in an e′ ($d_{x^2-y^2}$, d_{xy}) orbital, which reduces to 21a′ and 22a′ in C_s symmetry, as the nucleophile approaches the complex. At a metal–nucleophile distance of 3.0 Å, the electronic configuration for attack at an equatorial–equatorial edge (EE) of the trigonal-bipyramidal metal radical is $20a'^2 21a'^2 10a''^2 11a''^2 22a'^1$, while the electronic configuration for nucleophilic attack at a face or an axial–equatorial edge (AE) is $20a'^2 10a''^2 21a'^2 11a''^2 22a'^1$. The orbitals of interest in all three cases are the filled 20a′ (metal–phosphorus σ) and 21a′ (metal–carbon π, CO π*), derived from the metal e′ set, and the half-filled 22a′ (metal–phosphorus σ*). The energies and atomic character of the frontier orbitals for EE, AE, and facial (FAC) PH_3 attack at 17e D_{3h} $Mn(CO)_5$ are given in supplementary Tables IIIA–C, respectively.

Contour plots of the 20a′, 21a′, and 22a′ molecular orbitals are shown in Figures 7–9 for EE, AE, and FAC PH_3 attack, respectively. Parts A of Figures 7–9 show the 20a′ orbital for EE, AE, and facial PH_3 attack at the trigonal-bipyramidal metal radical. Note that EE and FAC attack provide for reasonable metal–nucleophile orbital overlap along the reaction path, while AE attack shows poor metal–nucleophile orbital overlap. For AE attack, it is apparent that the geometry does not provide access to the half-filled metal e′ orbital and that the hexacoordinate species formed is crowded. The half-filled 22a′ metal–phosphorus σ* orbitals (parts C of Figures 7–9) all show the expected de-stabilizing characteristics. The 22a′ for EE attack, however, offers two advantages over the 22a′ for both FAC and AE attack: (1) metal–carbon π overlap will help stabilize the orbital; (2) a carbonyl group is already trans to the entering PH_3 nucleophile and possesses metal–carbon σ* character, as would be expected for the leaving group in an S_N2 transition state. Comparison of the 21a′ orbitals in parts B of Figures 7–9 suggests attack by entering nucleophiles along an EE edge will produce the most favorable transition state. While the 21a′ orbital for EE attack
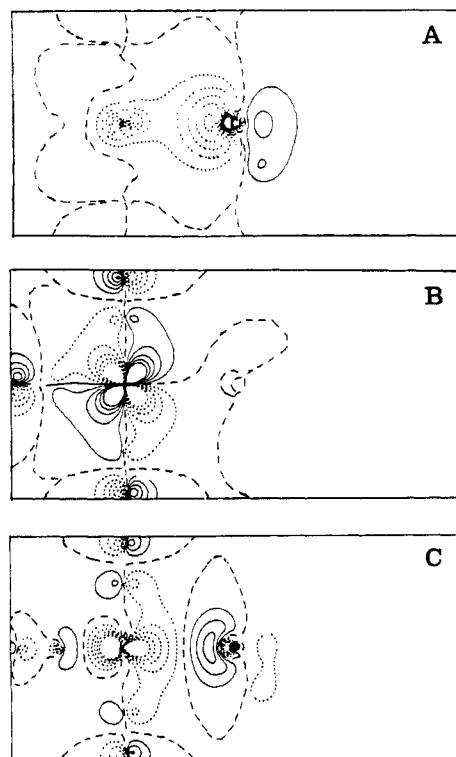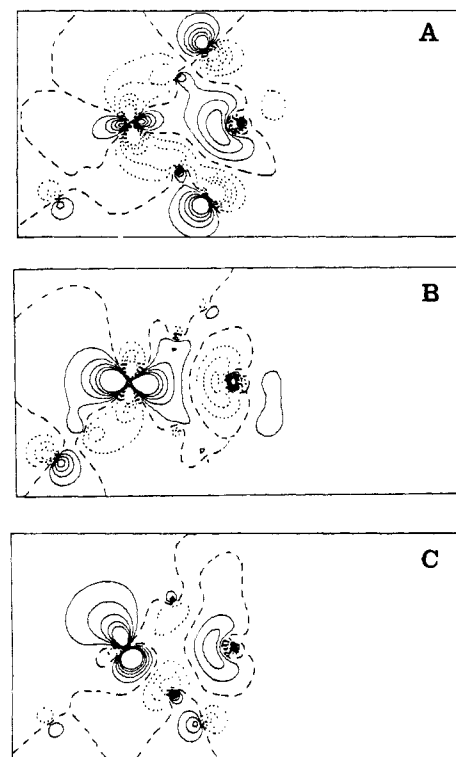

Figure 7. Contour plots of the three highest energy occupied a′ molecular orbitals for EE PH_3 attack at D_{3h} $Mn(CO)_5$ at a metal–nucleophile distance of 3.0 Å: (a) 20a′, (b) 21a′, and (c) 22a′. The interval between successive contours is 0.270 e/Å³.

Figure 8. Contour plots of the three highest energy occupied a′ molecular orbitals for AE PH_3 attack at D_{3h} $Mn(CO)_5$ at a metal–nucleophile distance of 3.0 Å: (a) 20a′, (b) 21a′, and (c) 22a′. The interval between successive contours is 0.270 e/Å³.

is completely metal d π–CO π* in character, the 21a′ orbitals for FAC and AE attack show some metal–phosphorus σ* character. This orbital interaction will destabilize a two-center three-electron bond because the 21a′ orbital is filled. Judging from these contour maps, nucleophilic attack along an edge in the equatorial plane
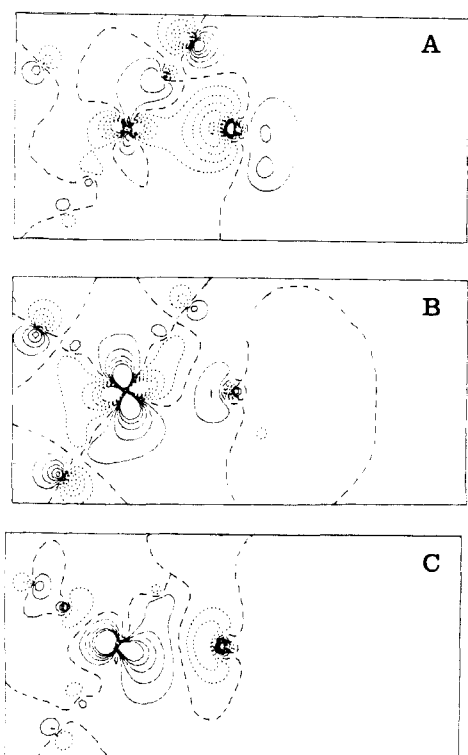
4948   *J. Am. Chem. Soc., Vol. 110, No. 15, 1988*

Therien and Trogler

Figure 9. Contour plots of the three highest energy occupied a′ molecular orbitals for FAC PH₃ attack at D_{3h} Mn(CO)₅ at a metal–nucleophile distance of 3.0 Å: (a) 20a′, (b) 21a′, and (c) 22a′. The interval between successive contours is 0.270 e/Å³.
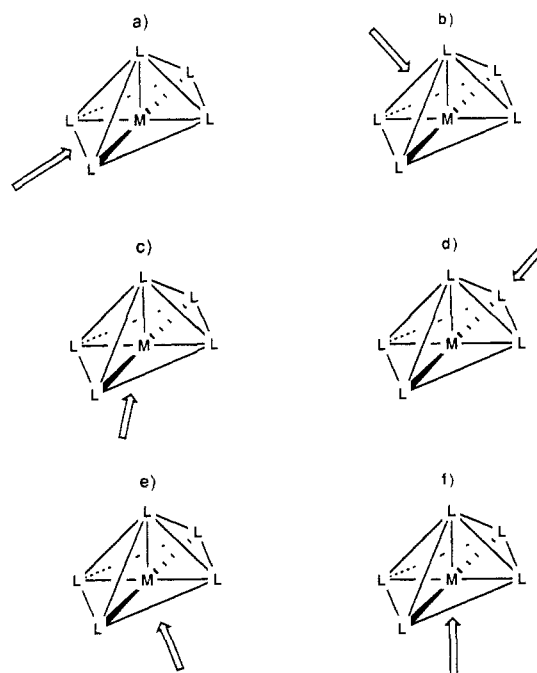

Figure 10. Six possible modes of nucleophilic attack at a square-pyramidal ML₅ metal radical complex: (a) attack along a vector bisecting an edge defined by two equatorial ligands (EE attack), (b) attack along a vector bisecting an edge defined by an axial ligand and an equatorial ligand (AE attack), (c) attack along a vector bisecting an edge defined by the half-filled metal a′ (d$_{z^2}$) orbital and an equatorial ligand (A′E attack), (d) attack along a vector passing through the center of a square-pyramidal face defined by the axial and two equatorial ligands (FAC attack), (e) attack along a vector passing through the center of a square-pyramidal face defined by the half-filled metal a′ (d$_{z^2}$) orbital and two equatorial ligands (FAC′ attack), and (f) attack along the C_4 axis (axial attack).

should provide the best S$_N$2 substitution pathway.

Six modes of nucleophilic attack can occur at a pentacoordinate square-pyramidal metal radical, such as 17e Mn(CO)₅ constrained to a C_{4v} geometry (Figure 10). They are (a) attack along a vector bisecting an edge defined by two adjacent equatorial ligands (EE), (b) attack along a vector bisecting an edge defined by an equatorial and the axial ligand (AE), (c) attack along a vector bisecting an edge defined by the half-filled metal d$_{z^2}$ orbital and an equatorial ligand (A′E), (d) attack along a vector passing through the center of a face defined by the axial ligand and two adjacent equatorial ligands (FAC), (e) attack along a vector passing through the center of a face defined by the half-filled metal d$_{z^2}$ orbital and two adjacent equatorial ligands (FAC′), and (f) attack along a vector bisecting the metal d$_{z^2}$ orbital (axial attack). Although all the models for hexacoordinate transition states depicted in Figure 10 possess formal C_s symmetry, note that A′E, FAC, FAC′, and EE attack approximate trigonal-prismatic geometries, while AE attack resembles bicapped-tetrahedral and axial-attack octahedral geometries. Throughout this study of nucleophilic attack at C_{4v} Mn(CO)₅, a CO$_{basal}$–Mn–CO$_{basal}$ angle of 164° is used in accord with previous experimental observations[29a] and theoretical considerations.[26b,31]

The odd electron in a 17e C_{4v} ML₅ complex resides in an orbital of a₁ symmetry with significant metal d$_{z^2}$ character. As the nucleophile approaches the complex, the symmetry reduces to C_s. At the metal–nucleophile distance of 3.0 Å, the electronic configuration of the six possible transition states or intermediates varies: for axial attack, the electronic configuration is 20a′²10a″²21a′²11a″²22a′¹; for AE attack, the electronic configuration is 20a′²10a″²11a″²21a′²22a′¹; for A′E attack the electronic configuration is 10a″²20a′²11a″²21a′²22a′¹; for EE, FAC, and FAC′ attack, the electronic configuration is 17a′²18a′²13a″²19a′²20a′¹. The orbitals of interest for AE, A′E, and axial attack are the 20a′, 21a′, and 22a′. The filled 20a′ orbital

is chiefly metal–phosphorus σ in character while the half-filled 22a′ orbital is metal–phosphorus σ*. The composition of 21a′ varies from being chiefly composed of metal d character (axial attack) to containing significant amounts of metal–phosphorus σ* character (AE, A′E attack). For FAC, FAC′, and EE attack we will consider the filled 17a′ (metal–phosphorus σ, metal–Cπ CO π*), the 19a′ (metal–carbon π, CO π*, metal–phosphorus σ*), and the half-filled 20a′ (metal–phosphorus σ*). The energies and atomic character of the frontier orbitals for AE, A′E, axial, FAC, FAC′, and EE attack of PH₃ at C_{4v} Mn(CO)₅ are given in supplementary Tables IVA–F, respectively.

Figures 11–13 show contour maps of the 20a′, 21a′, and 22a′ orbitals for AE, A′E, and axial PH₃ attack, respectively, at the square-pyramidal metal radical. Parts A of Figures 11–13 suggest that axial attack provides for the best metal–phosphorus σ bonding interaction for the 20a′ orbital, while parts B of Figures 11–13 illustrate unfavorable metal–phosphorus σ* interactions for the filled 21a′ when PH₃ attacks with an AE or A′E approach. Note that 21a′ for axial attack is chiefly metal d with some metal-C π and CO π* character. Although parts C of Figures 11–13 show half-filled 22a′ orbitals possessing varying amounts of metal–phosphorus σ* character, the effects of the filled 20a′ and 21a′ orbitals should dominate, leading to the conclusion that axial PH₃ attack at C_{4v} Mn(CO)₅ is favored.

Figures 14–16 show contour maps of the analogous orbitals (17a′, 19a′, and 20a′) for EE, FAC, and FAC′ attack of PH₃ at Mn(CO)₅. Contour plots in parts A of Figures 14–16 show that the 17a′ metal–phosphorus σ orbital exhibits the greatest metal–phosphorus orbital overlap for facial attack. Although the half-filled metal–phosphorus σ* orbital, 20a′ (parts C of Figures 14–16) shows minimal σ* character for EE attack (Figure 14C) and little for FAC (Figure 15C) and FAC′ (Figure 16C) attack, the filled 19a′ orbital shows appreciable metal–phosphorus σ* character for each of these three cases. This suggests a net Mn–P bond order of 0. Therefore, axial attack at C_{4v} Mn(CO)₅ should

(31) (a) Rossi, A. R.; Hoffmann, R. *Inorg. Chem.* **1975**, *14*, 365. (b) Burdett, J. K. *Inorg. Chem.* **1975**, *14*, 375. (c) Holmes, R. R. In *Progress in Inorganic Chemistry*; Lippard, S. J., Ed.; Wiley: New York, 1984; Vol. 32, 119. (d) Elian, M.; Hoffmann, R. *Inorg. Chem.* **1975**, *14*, 1058, and references therein.
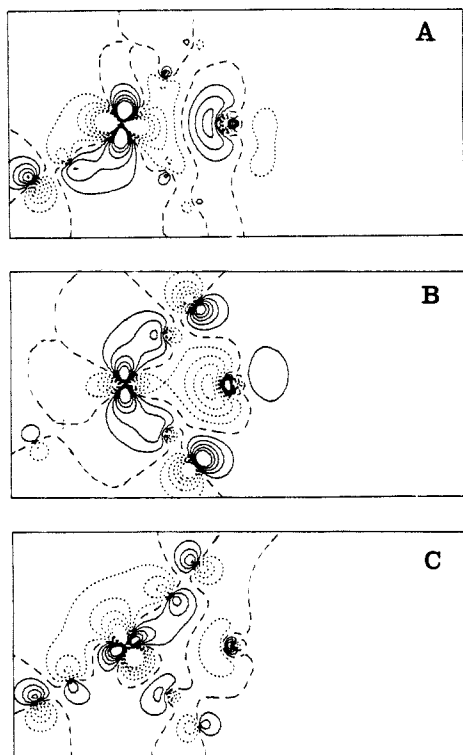
Figure 11. Contour plots of the three highest energy occupied a′ molecular orbitals for AE PH$_3$ attack at C_{4v} Mn(CO)$_5$ at a metal–nucleophile distance of 3.0 Å: (a) 20a′, (b) 21a′, and (c) 22a′. The interval between successive contours is 0.270 e/Å^3.
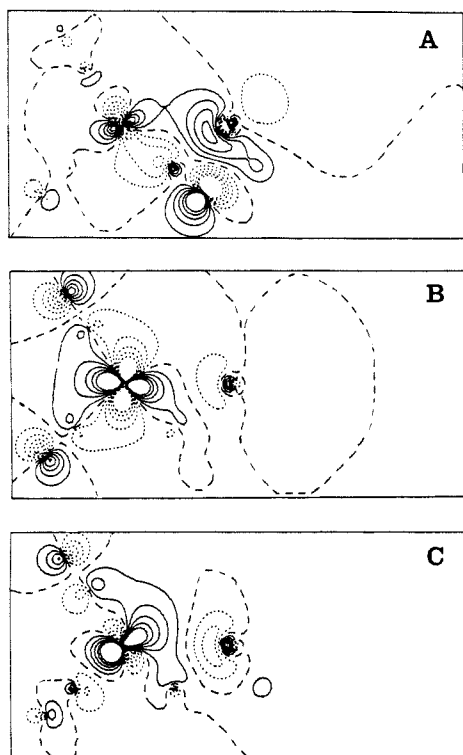

Figure 13. Contour plots of the three highest energy occupied a′ molecular orbitals for axial PH$_3$ attack at C_{4v} Mn(CO)$_5$ at a metal–nucleophile distance of 3.0 Å: (a) 20a′, (b) 21a′, and (c) 22a′. The interval between successive contours is 0.270 e/Å^3.

Figure 12. Contour plots of the three highest energy occupied a′ molecular orbitals for A′E PH$_3$ attack at C_{4v} Mn(CO)$_5$ at a metal–nucleophile distance of 3.0 Å: (a) 20a′, (b) 21a′, and (c) 22a′. The interval between successive contours is 0.270 e/Å^3.

Figure 14. Contour plots of the (a) 17a′, (b) 19a′, and (c) 20a′ orbitals for EE PH$_3$ attack at C_{4v} Mn(CO)$_5$ at a metal–nucleophile distance of 3.0 Å. The interval between successive contours is 0.270 e/Å^3.

provide the most stable hypervalent transition state and the most favorable S$_N$2 reaction pathway.

This result was expected, because the orbital containing the odd electron in 17e C_{4v} Mn(CO)$_5$ is largely metal d$_{z^2}$ in character and a square-pyramidal structure provides for great accessibility
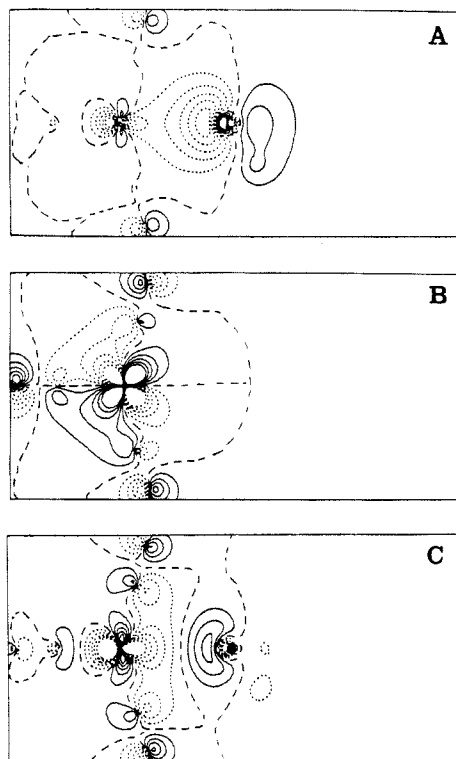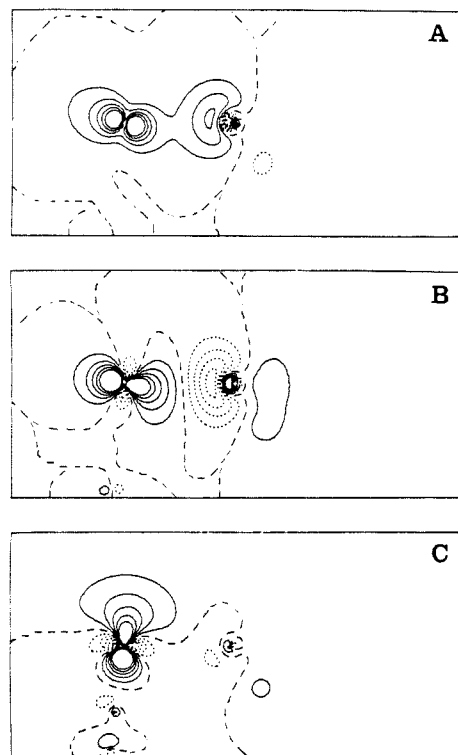
to this orbital when a nucleophile approaches the metal center from below the basal plane. It is interesting to note, however, that the contour maps of the six different modes of nucleophilic attack at a pentacoordinate 17e C_{4v} metal radical show that axial attack results in the *only* reaction path stabilized by a two-center three-electron bond.
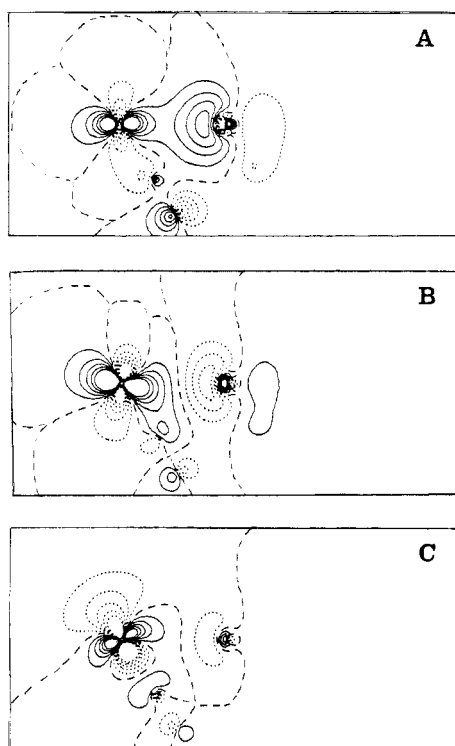
Figure 15. Contour plots of the (a) 17a′, (b) 19a′, and (c) 20a′ orbitals for FAC PH₃ attack at Mn(CO)₅ at a metal–nucleophile distance of 3.0 Å. The interval between successive contours is 0.270 e/Å³.
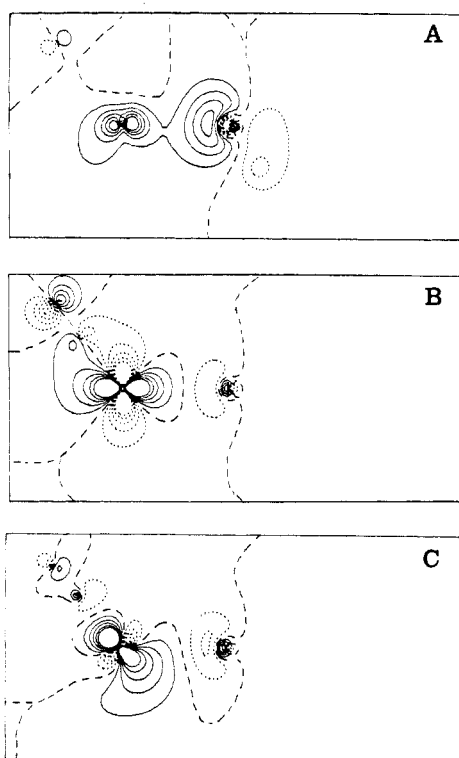

Figure 16. Contour plots of the (a) 17a′, (b) 19a′, and (c) 20a′ orbitals for FAC′ PH₃ attack at C_{4v} Mn(CO)₅ at a metal–nucleophile distance of 3.0 Å. The interval between successive contours is 0.270 e/Å³.

Tetracoordinate Metal Carbonyl Radicals. Although a few examples of 17e, four-coordinate metal carbonyl radicals are known,[32] in general these species are extremely unstable. For example, Co(CO)₄ is observed only at 6–15 K in CO matrices.[33]

(32) (a) Klein, H. F.; Karsch, H. H. *Chem. Ber.* **1975**, *108*, 944. (b) Rakowski, M. C.; Muetterties, E. L. *J. Am. Chem. Soc.* **1977**, *99*, 739.
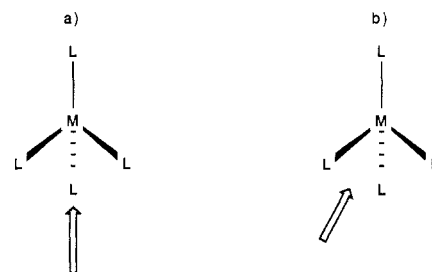
Figure 17. Two possible modes of nucleophilic attack at a tetrahedral ML₄ metal radical complex: (a) attack along a vector passing through the center of a tetrahedral face and (b) attack along a vector bisecting a tetrahedral edge.
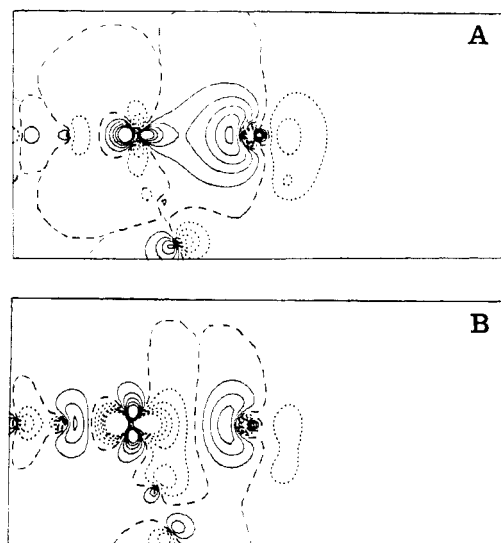

Figure 18. Contour plots of the two highest energy occupied molecular orbitals for facial PH₃ attack at T_d Co(CO)₄ at a metal–nucleophile distance of 3.0 Å: (a) 9a₁ and (b) 10a₁. The interval between successive contours is 0.270 e/Å³.

Like pentacoordinate radicals, these complexes exhibit high reactivity and participate in dimerization, atom-transfer, disproportionation, and catalytic[16,34,35] reactions. Spectroscopic evidence shows that Co(CO)₄ distorts slightly from tetrahedral (T_d) geometry and adopts a C_{3v} (pyramidal) structure in a solid-state CO matrix.[33] Throughout the course of this discussion we will consider Co(CO)₄ as the prototype for four-coordinate 17e metal radicals idealized to a tetrahedral structure.

As for 17e hexacoordinate transition-metal complexes, nucleophiles are constrained to two modes of attack at a tetrahedral ML₄ radical center: (1) attack along a vector bisecting an edge defined by any two ligands; (2) attack along a vector passing through the center of a trigonal face defined by any three ligands (Figure 17). Facial attack by PH₃ produces a C_{3v} transition-state model resembling a distorted trigonal-bipyramidal structure, while edge attack gives a species with C_s symmetry, a trapezoidal pyramid.

The odd electron in 17e T_d Co(CO)₄ resides in the metal-localized e orbital, as expected for a d⁹ tetrahedral complex. At a metal–nucleophile distance of 3.0 Å, the electronic configuration for PH₃ attack at a tetrahedral face is 9a₁²8e⁴9e⁴10a₁¹, while the electronic configuration for nucleophilic attack at an edge of the tetrahedron is 16a′²9a″²17a′²10a″²18a′²19a′¹. For facial PH₃ attack, the orbitals containing significant metal and phosphorus σ character are 9a₁ (metal–phosphorus σ) and the singly occupied 10a₁ (metal–phosphorus σ*, metal–carbon σ*, CO σ). For edge

(33) Hanlan, L. A.; Huber, H.; Kundig, E. P.; McGarvey, B. R.; Ozin, G. A. *J. Am. Chem. Soc.* **1975**, *97*, 7054.

(34) (a) Feder, H. M.; Halpern, J. *J. Am. Chem. Soc.* **1975**, *97*, 7187. (b) Sweany, R. Halpern, J. *Ibid* **1977**, *99*, 8335.

(35) (a) Rathke, J. W.; Feder, H. M. *J. Am. Chem. Soc.* **1978**, *100*, 3623. (b) Azran, J. Orchin, M. *Organometallics* **1984**, *3*, 197.

Table III. Atomic Character of Frontier Orbitals for Facial PH_3 Attack at T_d $Co(CO)_4$ (Cobalt–Phosphorus Distance 3.0 Å)

orbital	energy, eV	orbital character	% contribution from atoms						
			Co	C^b	O^b	C^c	O^c	P	H
12e	-4.99	$d_{x^2-y^2}$, d_{xy}, d_{yz}, d_{xz}	11	44	28	11	5	0	0
11a₁	-5.06	d_{z^2}	17	8	2	42	25	5	1
2a₂	-5.16		0	0	0	64	36	0	0
11e	-5.18	$d_{x^2-y^2}$, d_{xy}, d_{yz}, d_{xz}	16	6	3	48	25	0	1
10e	-5.39	$d_{x^2-y^2}$, d_{xy}, d_{yz}, d_{xz}	11	0	0	55	33	1	1
10a₁^a	-8.11	d_{z^2}	40	14	2	18	4	16	5
9e	-8.94	$d_{x^2-y^2}$, d_{xy}, d_{yz}, d_{xz}	56	4	4	26	10	0	0
8e	-10.33	$d_{x^2-y^2}$, d_{xy}, d_{yz}, d_{xz}	86	1	3	2	9	0	0
9a₁	-10.92	d_{z^2}	12	4	0	4	13	62	6
7e	-13.01		1	0	0	3	4	46	46
6e	-14.20		3	20	63	5	9	0	0
8a₁	-14.26	d_{z^2}	24	29	28	11	8	0	0
5e	-14.35	$d_{x^2-y^2}$, d_{xy}, d_{yz}, d_{xz}	12	3	9	38	37	0	0

^{a} Denotes highest occupied orbital. ^{b} Denotes atom trans to entering nucleophile. ^{c} Denotes atoms defining the tetrahedral face.

Table IV. Atomic Character of Frontier Orbitals for Edge PH_3 Attack at T_d $Co(CO)_4$ (Cobalt–Phosphorus Distance 3.0 Å)

orbital	energy, eV	orbital character	% contribution from atoms									
			Co	C^b	O^b	C^b	O^b	C^c	O^c	P	H^d	H
23a'	-1.47	d_{z^2}, $d_{x^2-y^2}$, d_{xy}	13	26	15	19	10	5	1	6	4	1
14a''	-2.00	d_{yz}, d_{xz}	15	24	16	16	9	13	7	0	0	0
22a'	-2.07	d_{z^2}, $d_{x^2-y^2}$, d_{xy}	18	10	2	1	0	44	24	0	0	0
13a''	-2.08		2	10	5	9	4	42	26	0	0	0
21a'	-2.11	d_{z^2}, $d_{x^2-y^2}$, d_{xy}	17	1	0	8	3	43	27	0	0	0
12a''	-2.14		0	3	1	12	6	48	28	1	1	0
11a''	-2.23	d_{yz}, d_{xz}	18	16	8	21	10	16	6	2	2	0
20a'	-2.80		7	21	15	24	15	2	1	7	3	5
19a'^{a}	-5.38	d_{z^2}, $d_{x^2-y^2}$, d_{xy}	50	12	1	11	1	13	4	3	4	2
18a'	-5.85	d_{z^2}, $d_{x^2-y^2}$, d_{xy}	53	10	3	11	2	11	8	0	0	0
10a''	-5.98	d_{yz}, d_{xz}	56	4	5	4	4	21	5	0	0	0
17a'	-7.07	d_{z^2}, $d_{x^2-y^2}$, d_{xy}	79	0	0	0	0	4	8	7	1	0
9a''	-7.22	d_{yz}, d_{xz}	86	1	3	1	3	2	5	0	0	0
16a'	-8.41	d_{z^2}, $d_{x^2-y^2}$, d_{xy}	18	4	14	5	15	0	0	35	6	2
15a'	-10.40		7	8	14	8	15	0	0	17	11	20
8a''	-11.14	d_{yz}, d_{xz}	12	2	7	4	12	19	11	14	17	0
7a''	-11.20	d_{yz}, d_{xz}	10	3	6	2	4	31	19	11	13	0
14a'	-11.26	d_{z^2}, $d_{x^2-y^2}$, d_{xy}	21	20	23	2	1	17	12	3	0	0
13a'	-11.31	d_{z^2}, $d_{x^2-y^2}$, d_{xy}	16	9	8	29	22	9	4	3	0	1

^{a} Denotes highest occupied orbital. ^{b} Denotes atoms defining the tetrahedral edge. ^{c} Denotes additional atoms related by the mirror plane. ^{d} Denotes hydrogens related by the mirror plane.

attack, the orbitals we will consider are 16a' (metal–phosphorus σ, metal–carbon π, CO π*), 17a' (metal–phosphorus σ*), and the half-occupied 19a' (metal–carbon π*, CO π, metal–phosphorus σ*). The energies and atomic character of the frontier orbitals for facial and edge PH_3 attack at 17e T_d $Co(CO)_4$ are given in Tables III and IV, respectively.

Contour plots of the 9a₁ and 10a₁ orbitals for facial attack are shown in Figure 18. The 9a₁ orbital of Figure 18A shows a relatively uncrowded model for a hypervalent transition state with good metal–phosphorus σ overlap. Note that the trans metal–carbon bond possesses significant σ* character in the pseudo-trigonal-bipyramidal transition state, which resembles a nucleophilic displacement at tetrahedral carbon. The HOMO, the half-filled 10a₁ orbital (Figure 18B), shows substantial metal–phosphorus σ* and metal–(trans) carbon σ* character.

Figure 19 shows the relevant orbitals for edge attack at the tetrahedron. Like the metal–phosphorus σ bonding orbital for facial attack in Figure 18A, good overlap is observed for the 16a' orbital in Figure 19A. The chief energetic difference between the trigonal-bipyramidal transition-state model arising from facial attack and the trapezoid-pyramidal transition-state model arising from edge attack is apparent in Figure 19B. The filled 17a' orbital shown here has significant metal–phosphorus σ* character, which implies a net bond order of 0 between the metal and nucleophile. Even though the half-filled 19a' orbital of Figure 19C has decreased metal–phosphorus σ* character relative to Figure 19B, this should have a minimal influence on the total energy of a C_s transition state arising from edge attack. On the basis of the contour plots, one concludes that nucleophilic attack should occur at a face rather than at an edge of the tetrahedron.

Conclusion

In each of the homoleptic 17e metal carbonyl radical structures we have examined (octahedral, trigonal bipyramidal, square pyramidal, and tetrahedral), a two-center three-electron bond can develop by nucleophilic attack at an appropriate edge or face of the given polyhedra. These studies suggest that only one particular mode of attack will lead to a transition state or intermediate stabilized by a two-center three-electron bond for trigonal-bipyramidal, square-pyramidal, and tetrahedral ML_n radicals. While both edge and facial nucleophilic attack at an octahedral metal radical may lead to a hypervalent transition state with a net metal–nucleophile bond order of $^1/_2$, this work suggests that the species formed by attack at a face is slightly favored. A common feature of the homoleptic metal carbonyl radical systems examined is they all possess a sterically accessible orbital containing the odd electron. Thus, not all electron-deficient metal radicals need be substitution labile: Such is the case for $(C_5H_7)_2VCO^{8c}$ and $Mn(\eta^4\text{-butadiene})L^{36}$ complexes, where the orbital containing the odd electron was shown to be shielded from nucleophilic attack by the polyolefin ligands.

The models for 19e hypervalent transition states discussed are characterized by the presence of an odd electron in a σ* orbital, formed from the weak bond between the metal and the entering nucleophile. This electronic stabilization provides the simplest rationale for the enhanced rate of nucleophilic substitution observed in 17e metal-centered radicals. It is important, however, to distinguish these 19e transition states from ground-state 19e

(36) Harlow, R. L.; Krusic, P. J.; McKinney, R. J.; Wreford, S. S. *Organometallics* **1982**, *1*, 1506.
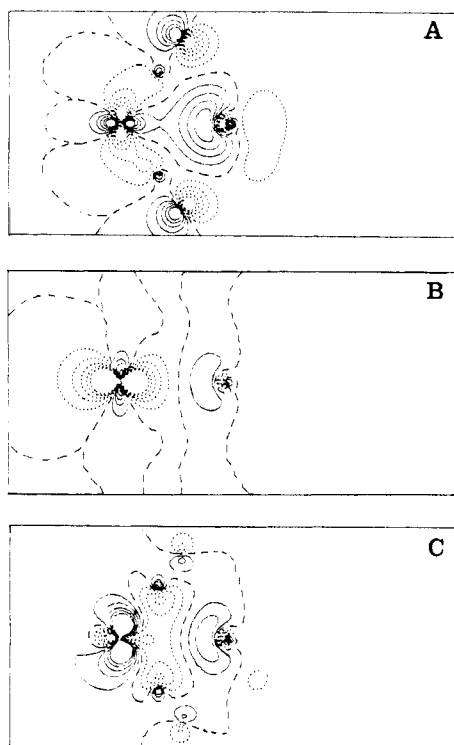
Figure 19. Contour plots of the (a) 16a′, (b) 17a′, and (c) 19a′ orbitals for edge PH_3 attack at T_d $Co(CO)_4$ at a metal–nucleophile distance of 3.0 Å.

Table V. Calculated Spin Distribution and Orbital Populations in D_{3h} $Mn(CO)_5$

atom	orbital	occupation[b]	spin density
Mn	3d	6.07	-0.83
	4s	-0.04	0.08
	4p	0.29	-0.25
	pop chg = +0.68		
	∫chg = 0.96		
C[a]	2s	1.34	0.00
	2p	2.47	0.03
	pop chg = 0.20		
	∫chg = 0.16		
O	2s	1.82	0.00
	2p	4.52	0.00
	pop chg = -0.33		
	∫chg = -0.36		

[a] The values for axial and equatorial CO groups are averaged. [b] pop chg = Mulliken type charge; ∫ chg = volume-integrated charge.

complexes and from 19e species formed via one-electron reduction of coordinatively saturated 18e compounds.

As ground-state 17e complexes are susceptible to nucleophilic attack, ground-state 19e complexes are susceptible to dissociative ligand substitution.[3e,37] The balance between nonbonded repulsions and electronic stabilization of the 3e bond will determine whether 19e species are intermediates and lie in a potential well along the reaction coordinate or whether they are transition states and lie at an energy maximum.

Reduction of a saturated 18e complex such as $Fe(CO)_5$ results in the formation of a 19e species. Here the odd electron may reside in a covalent metal CO π^* orbital,[38] a case clearly different from the 19e species formed via nucleophilic attack at a 17e metal-centered radical. Tables V and VI give the calculated spin and orbital populations for a model 17e metal-centered radical, D_{3h} $Mn(CO)_5$, and for the 19e hypervalent complex formed when PH_3 attacks the metal radical along an equatorial–equatorial (EE) edge.

(37) Summers, D. P.; Luong, J. C.; Wrighton, M. S. *J. Am. Chem. Soc.* **1981**, *103*, 5238.

(38) Holland, G. F.; Manning, M. C.; Ellis, D. E.; Trogler, W. C. *J. Am. Chem. Soc.* **1983**, *105*, 2308.

Table VI. Calculated Spin Distribution and Orbital Populations for Equatorial–Equatorial Edge PH_3 Attack at D_{3h} $Mn(CO)_5$ (Metal–Phosphine Bond Distance 2.8 Å)

atom	orbital	occupation	spin density
Mn	3d	6.10	-0.87
	4s	-0.03	0.35
	4p	0.34	-0.40
	pop chg = 0.59		
	∫chg = 1.15		
C[a]	2s	1.32	0.00
	2p	2.51	0.02
	pop chg = 0.17		
	∫chg = 0.01		
O	2s	1.82	0.00
	2p	4.52	0.01
	pop chg = -0.34		
	∫chg = -0.31		
P	3s	1.68	-0.20
	3p	3.34	-0.14
	3d	-0.03	0.08
	pop chg = -0.02		
	∫chg = 2.13		
H	1s	0.90	0.02
	pop chg = 0.10		
	∫chg = -0.59		

[a] The values of all carbonyls were averaged.

(The Mn–phosphorus bond distance in this model for an associative transition state is 3.0 Å.) Similar to spin-polarized SCF–Xα–DV calculations for other metal-centered radicals,[26a] Table V shows that most of the unpaired electron spin density resides on the Mn atom in D_{3h} $Mn(CO)_5$. Carrying out a spin-polarized calculation for the model hypervalent 19e transition state (Table VI) reveals that most of the unpaired electron density still resides on the Mn atom with some delocalization onto phosphorus; however, little spin density appears on the carbonyl carbon or oxygen atoms. This lack of transfer of spin density onto the ligands contrasts with recent work by Kochi[3e] showing that 19e species formed via reduction of 18e complexes can impart radical reactivity to the ligands. For example, the 19e anion radicals $Fe(CO)_5^-$ and $Cr(CO)_6^-$, where the electron occupies a CO π^* orbital or a σ^* orbital of the M–CO bond, abstract H atoms from donors such as $HSnBu_3$ to give metal formyls as well as dissociate CO; thus, reaction paths can differ for 19e metal radicals depending on the distribution of the odd electron.

Computational Details

Electronic structure calculations were performed with a DEC-VAX 11/750 minicomputer by the self-consistent field–discrete variational–Xα method (SCF–Xα–DV).[39] Numerical atomic orbitals from exact Hartree–Fock–Slater calculations were used as basis functions, assuming the α values of Schwartz.[40] For metal atoms, the atomic orbitals through 4p were included; for P, the atomic orbitals through 3d were used as a basis; for C and O, a minimal 1s, 2s, 2p basis was used; for H, a 1s function was used. Core orbitals (1s, ..., 3p for M; 1s, 2s, 2p for P; and 1s for C and O) were frozen and orthogonalized against valence orbitals. The Mulliken[41] scheme was used to compute atomic orbital populations. The molecular Coulomb potential was calculated with a least-squares fit[42] of the model electron density to the true density. A total of 7 radial degrees of freedom was allowed in the expansion of the density, in addition to the radial atomic densities. The molecular exchange potentials used were α = 0.71556, 0.71252, and 0.7100 for V, Mn, and Co atoms, respectively. Spin-restricted calculations were performed to deduce qualitative bonding features of the 19e transition states, while spin-polarized calculations[44] provided information regarding electron spin distribution in these species.

Phosphine was chosen as a computationally accessible nucleophile for these studies. The assumed P–H bond length was 1.415 Å.[43] For oc-

(39) (a) Ellis, D. E.; Painter, G. S. *Phys. Rev. [Sect.] B* **1970**, *2*, 2887. (b) Delley, B.; Ellis, D. E. *J. Chem. Phys.* **1982**, *76*, 1949.

(40) Schwartz, K. *Phys. Rev. [Sect.] B* **1972**, *4*, 2466.

(41) Mulliken, R. S. *J. Chem. Phys.* **1955**, *23*, 1833.

(42) Delley, B.; Ellis, D. E.; Freeman, A. J.; Barends, E. J.; Post, D. *Phys. Rev. [Sect.] B.* **1983**, *27*, 2132.

(43) Norman, J. G., Jr. *Inorg. Chem.* **1977**, *16*, 1328.

(44) Bellard, S.; Rubinson, K. A.; Sheldrick, G. M. *Acta Crystallogr., Sect. B: Struct. Crystallogr. Cryst. Chem.* **1979**, *35*, 271.

tahedral V(CO)$_6$, the V–C and C–O bond lengths were taken to be 2.001 and 1.128 Å, respectively, from published X-ray data.[44] The structures used for pentacoordinate Mn(CO)$_5$ were idealized D_{3h} and C_{4v} geometries; the C_{4v} structure for Mn(CO)$_5$ was taken to have a CO$_{basal}$–Mn–CO$_{basal}$ angle of 164°, on the basis of previous experimental observations[29a] and theoretical considerations.[26b,31] The Mn–C and C–O bond distances were taken to be 1.855 and 1.129 Å, respectively, from the published X-ray data of Mn$_2$(CO)$_{10}$.[45] The Co–C and C–O bond lengths used for Co(CO)$_4$ in the ideal tetrahedral geometry were 1.797 and 1.168 Å on the basis of the X-ray data for Co$_2$(CO)$_8$.[46]

For all the electronic structure calculations of the hypothetical models for 19e transition states, a coordinate system was used such that PH$_3$ approached the metal center along the z axis. The metal carbonyl complex was rotated in space to provide for nucleophilic attack by PH$_3$ at the appropriate edge or face of the polyhedron such that the xz plane

always functioned as a plane of symmetry, allowing for easy comparison of the contour maps generated. The relative orbital energies for calculations at different metal–nucleophile distances can vary by ±0.5 eV from errors in the numerical integration scheme. Therefore, the Walsh diagrams were constructed by using a core orbital of oxygen on the remote carbonyl ligands as an internal reference to compare orbital energies vs metal–nucleophile distance. The success of this procedure is evident in Figure 2 where the noninteracting 12e orbital energy remains constant while the energies of the interacting 10a$_1$ and 11a$_1$ orbitals vary considerably.

Supplementary Material Available: Tables of atomic character of frontier orbitals (24 pages). Ordering information is given on any current masthead page.

(45) Churchill, M. R.; Amoh, K. N.; Wasserman, H. J. *Inorg. Chem.* **1981,** *20,* 1609.

(46) Sumner, G. G.; Klug, H. P.; Alexander, L. E. *Acta Crystallogr.* **1964,** *17,* 732.

Empirical Potential Energy Surfaces Relating Structure and Activation Energy. 1. Metallacyclopentene Ring Inversion in (*s-cis*-η⁴-Butadiene)metallocene Complexes and Related Compounds

Hans-Beat Bürgi* and Katharina C. Dubler-Steudle

Contribution from the Laboratory for Chemical and Mineralogical Crystallography, University of Berne, CH-3012 Berne, Switzerland. Received June 23, 1987

Abstract: X-ray structural data for (*s-cis*-η⁴-butadiene)metallocene complexes and activation barriers for metallacyclopentene ring inversion in these compounds were retrieved from the literature and analyzed by principal-component analysis. It is found that the metallacyclopentene rings can be arranged into a sequence in which the bite size of the butadiene ligand decreases continuously, the envelope conformation of the ring becomes increasingly planar, and the free energy of activation for ring inversion decreases. If the sequence of observed structures is interpreted as mapping the reaction pathway and if for a molecule with equilibrium structure x_0 the energy profile along the reaction coordinate x is of the form $\Delta E = ax^4 - 2ax_0^2x^2$, it may be shown that $\Delta E^* = -ax_0^4$. The experimental data closely follow such a relationship, $\Delta G^* = -ax_0^4$. This finding establishes a relationship between change in equilibrium structure, change in activation energy, and energy profile for an individual molecule. The results represent a quantitative illustration of Hammond's postulate based exclusively on experimental structural and kinetic data.

Structural Correlations. A commonly used method to gain chemical information is to study a basic molecular fragment in different environments. In particular, variation of substituents provides a basis for discerning electronic and steric effects on the properties of the fragment. This general idea has been applied over the last 15 years to the analysis of changes in structural parameters of molecules containing the same basic fragment. It has been found that changes in distances and angles are often correlated and that this correlation can be interpreted in terms of structural reaction coordinates for such diverse processes as conformational interconversions, bond-breaking and bond-making processes.[1] The influence of varying environments may be considered as a perturbation on the energy surface of the basic fragment,[2] which preserves its basic features of minima, valleys, and transition states. In the last few years both structural and kinetic data have become available for sufficiently large families of related molecules. This opens up the possibility of enlarging

the scope of structural reaction pathway studies by adding the dimension of energy. In this paper results of X-ray crystal structure determinations and of temperature-dependent NMR experiments are combined with the aim of understanding an observed, rather pronounced dependence of activation energy on small changes in observed molecular structure.

Automerization of Zirconocene and Hafnocene Complexes. (*s-cis*-η⁴-Butadiene)zirconocene and -hafnocene complexes have been investigated and described in the literature by Erker and co-workers.[3–6] Temperature-dependent NMR spectroscopy in solution shows dynamic behavior, which has been interpreted in terms of a ring-inversion mechanism[3,5] (Scheme I). Structural data are available for 12 related compounds,[3–8] 9 zirconocene and

(1) For a review, see: Bürgi, H. B.; Dunitz, J. D. *Acc. Chem. Res.* **1983,** *16,* 153–161.

(2) Or, more accurately, on a reference molecule suitably chosen from a family of related molecules.

(3) Erker, G.; Engel, K.; Krüger, C.; Chiang, A.-P. *Chem. Ber.* **1982,** *115,* 3311–3323.

(4) Erker, G.; Engel, K.; Krüger, C.; Müller, G. *Organometallics* **1984,** *3,* 128–133.

(5) Krüger, C.; Müller, G.; Erker, G.; Dorf, U.; Engel, K. *Organometallics* **1985,** *4,* 215–223.

(6) Erker, G.; Engel, K.; Krüger, C.; Tsay, Y.-H.; Samuel, E.; Vogel, P. Z. *Naturforsch., B: Anorg. Chem., Org. Chem.* **1985,** *40B,* 150–157.